Simplified Determination of the Thermal Resistance of Vertical-Cavity Surface-Emitting Lasers

Markus Daubenschüz

We present a novel approach to determine the thermal resistance and the internal temperature of vertical-cavity surface-emitting lasers (VCSELs) based on easily accessible laser parameters. The described method does not use any empirical parameters or pulsed measurements that are often mentioned in literature. We explain how to determine the thermal resistance and show the computation of the internal temperature for any operation point. Furthermore the data evaluation can be used for characteristic parameter extraction that enables us to establish an isothermal modeling of the VCSEL operation curves.

1. Introduction

VCSELs are key optoelectronic devices for optical sensing and data communication in high-performance computing, data centers, and in-building networks [1, 2]. The performance of such lasers depends on numerous design parameters. To develop and optimize next-generation VCSELs with data rates of 28 Gbit/s and above [3, 4] or to enable new sensing applications, an accurate knowledge about current flow and heat generation inside the device is inevitable. High average internal temperatures T_i in the laser cavity are a major problem, causing, e.g., a drop in conversion efficiency and reduced lifetimes. For datacom VCSELs T_i easily rises since higher-speed lasers need higher currents to reach the required bandwidth. In general, VCSELs are often used in environments where active cooling is not permitted due to the involved power dissipation and cost. Different approaches have been demonstrated to decrease the internal temperature by a reduction of the thermal resistance [5, 6] or by minimizing the optical absorption [7] and series resistances [8]. To compare the impact of different designs, an accurate determination of T_i is required. An externally measurable parameter that is exclusively related to the temperature distribution inside the laser is the change of the resonance wavelength with temperature. For VCSELs with an emission wavelength in the 800–1000 nm range, a mode shift of $\mathrm{d}\lambda/\mathrm{d}T \approx 0.07\,\mathrm{nm/K}$ [9] is found. This value can be used to estimate the temperature increase directly form the measured spectral red-shift. Another common method to compute T_i is the determination of the thermal resistance

$$R_\mathrm{Th} = \frac{\Delta T}{\Delta P_\mathrm{diss}}\,, \tag{1}$$

which relates the average temperature change ΔT in the laser cavity to a change ΔP_diss of the dissipated power. For this purpose, the VCSEL is typically driven with electrical

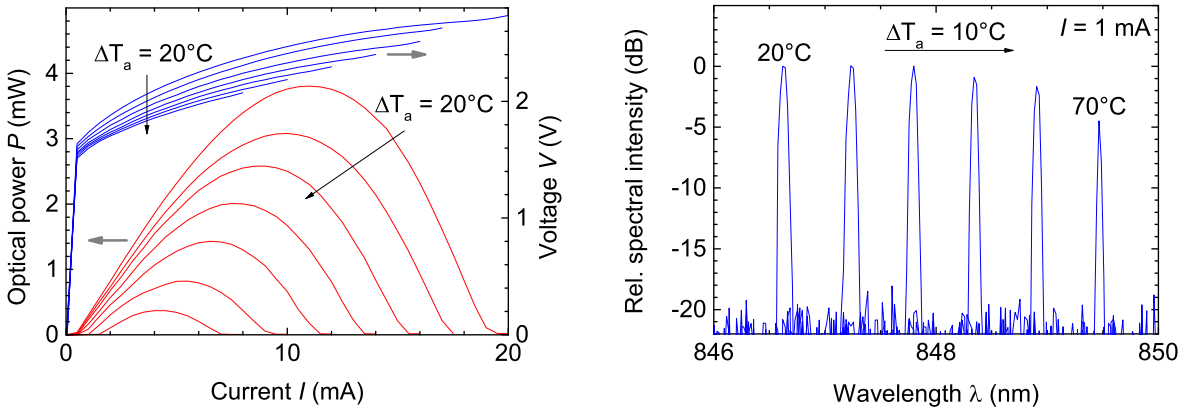

Fig. 1: Temperature-dependent light–current–voltage characteristics of a VCSEL with an active diameter $D_{\mathrm{ac}} = 4\,\mu\mathrm{m}$ for $T_{\mathrm{a}} = 0°\mathrm{C}$ to $120°\mathrm{C}$ in steps of $20°\mathrm{C}$ (left) and optical spectra of the same laser at different T_{a} and $I = 1\,\mathrm{mA}$ current (right).

pulses up to a few hundred nanoseconds [10], namely shorter than the thermal time constant which is in the range of some microseconds [11]. With this method, no internal heating of the VCSEL by the dissipated power arises and thereby no thermal wavelength shift appears. Pulsed operation thus allows to separate the influence of internal and external heating. The wavelength shift is then only induced by a change of the ambient temperature T_{a}. A series of such measurements results in the above-mentioned $\mathrm{d}\lambda/\mathrm{d}T$. As will be seen later, the VCSEL behaves differently for uniform heating and for internal heating by a dissipated power density profile. The drawback of pulsed measurements is the need for high-speed equipment. In this article we briefly describe the thermal influence on the laser characteristics and show the novel procedure of determining the thermal resistance and internal temperature. The analysis of T_{i} enables us to establish an isothermal model by which we can extract important static laser parameters dependent on the internal temperature.

2. Thermal Resistance

As can be seen in Fig. 1 (left), the operation curves of a VCSEL or of a laser diode in general are highly temperature-dependent. They are influenced by the ambient temperature as well as the internal temperature, which is related to several different mechanisms of power dissipation [12]. The effects can be classified into linear power dissipation (absorption, carrier thermalization, carrier leakage, and spontaneous carrier recombination) and quadratic power dissipation across the series resistance [13]. An increase of the internal temperature T_{i} leads to a change of different internal parameters that result in the case of Fig. 1 in an increase of the threshold current I_{th}, a decrease of the slope efficiency SE, and reductions of the kink voltage V_{k} and the differential resistance $R_{\mathrm{d}} = \mathrm{d}V/\mathrm{d}I$. All of these changes are indirectly related to T_{i} and cannot be used to determine the internal temperature.

As mentioned before, one measurable parameter that exclusively depends on the temperature profile is the resonance wavelength λ of the VCSEL. With an increase of T_{i} or

T_a one observes a so-called red-shift of the emission spectrum to higher wavelengths, as displayed in Fig. 1 (right). The shift is induced by a temperature-related change of the refractive indices $\bar{n}$ of the semiconductor materials and by the thermal expansion of the epitaxial layers and can be expressed as

$$\frac{1}{\lambda}\frac{\mathrm{d}\lambda}{\mathrm{d}T} = \frac{1}{\bar{n}}\frac{\mathrm{d}\bar{n}}{\mathrm{d}T} + \frac{1}{L}\frac{\mathrm{d}L}{\mathrm{d}T}\,, \tag{2}$$

which follows from the laser resonance condition. Both $\mathrm{d}\bar{n}/\mathrm{d}T > 0$ and $\mathrm{d}L/\mathrm{d}T > 0$. The second term on the right is more than an order of magnitude smaller than the first one.

The continuous-wave (cw) measurements of Fig. 1 were performed at wafer level on GaAs-based VCSELs with an operation wavelength close to 850 nm and varying active diameters D_ac. The active region of the VCSELs contains three GaAs quantum wells, and the top and bottom Bragg mirrors have 21 and 37.5 layer pairs, respectively. The LIV and spectral data were taken with a fully automated setup including a precise temperature-controlled wafer chuck. For a measurement range from -10 to 140°C the curves were recorded in steps of 5°C. The output power was measured with a calibrated Si photodiode housed in an integrating sphere. The spectral measurements were done with a grating spectrometer with wavelength steps of 22 pm, from which the measurable temperature resolution can be estimated as 0.3 K when $\mathrm{d}\lambda/\mathrm{d}T \approx 0.07\,\mathrm{nm/K}$.

The dissipated power needed for the determination of R_Th is defined as

$$P_\mathrm{diss} = P_\mathrm{el} - P = IV\,(1 - \eta_\mathrm{c}) \tag{3}$$

with the electrical power P_el, the optical output power P, the injected current I, the voltage drop V over the VCSEL, and the conversion efficiency $\eta_\mathrm{c} = P/P_\mathrm{el}$. In Fig. 2 we show measurements of the peak wavelength λ_p of the fundamental LP_{01} mode over P_diss for the single-mode VCSEL from Fig. 1. One can clearly see a linear relation of λ_p and P_diss in the working range of the VCSEL for all ambient temperatures. This would also be true for higher-order transverse modes [14]. Nevertheless in the following we will restrict ourselves to the fundamental mode. In the analysis, this linear behavior of the mode shift versus P_diss is used to determine the thermal resistance R_Th of the laser. From (1) we can also write R_Th as [9]

$$R_\mathrm{Th} = \frac{\Delta T}{\Delta P_\mathrm{diss}} = \frac{\Delta\lambda/\Delta P_\mathrm{diss}}{\Delta\lambda/\Delta T} = \frac{C_1}{C_2} \tag{4}$$

with the parameters $C_1 = \Delta\lambda/\Delta P_\mathrm{diss}$ and $C_2 = \Delta\lambda/\Delta T$ for the wavelength shifts with dissipated power and ambient temperature, respectively. The parameter C_2 is mainly related to the change $\mathrm{d}\bar{n}/\mathrm{d}T$ of the refractive indices with temperature (see (2)) and — to avoid self-heating — must be determined with pulsed measurements or the aforementioned estimated value for $\mathrm{d}\lambda/\mathrm{d}T$. Our approach eliminates these difficulties or uncertainties in the following way: with simple linear extrapolations we can identify the wavelengths λ_0 of the LP_{01} mode without internal heating ($P_\mathrm{diss} = 0\,\mathrm{mW}$) for all T_a. The data points correspond to the LP_{01} peak wavelengths of the laser in pulsed operation. The plot $\lambda_0 = \lambda_0\,(T_\mathrm{a})$ yields a linear relationship with a slope of $\mathrm{d}\lambda_0/\mathrm{d}T_\mathrm{a} = 57\,\mathrm{pm/K}$, as shown in Fig. 3 (left). As expected, for the same epitaxial design we find the same slope for

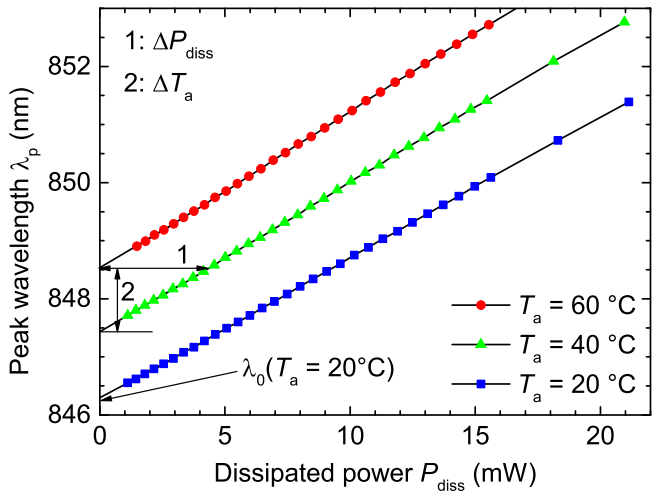

Fig. 2: Peak wavelength λ_p versus dissipated power P_diss for different ambient temperatures T_a. The labels '1' and '2' indicate the required changes of P_diss and T_a in (4).

all other values of D_ac. As can be seen in Fig. 2, λ_p increases linearly with P_diss, i.e., no curvature is seen even for high dissipated power. However, the slope of the straight lines increases with T_a. We find values of $\mathrm{d}\lambda/\mathrm{d}P_\mathrm{diss} = 0.24\,\mathrm{nm/mW}$ for $T_\mathrm{a} = 20°\mathrm{C}$ to 0.32 nm/mW for 100°C. To deduce the thermal resistance in (4) we need associated values of ΔT and ΔP_diss. For our analysis we are using the fact that one gets the same emission wavelength for the same average internal temperature of the VCSEL, irrespective of T_a or P_diss being the origin. With the temperature-controlled wafer chuck we generate a $\Delta T = \Delta T_\mathrm{a}$ that is labeled with '2' in Fig. 2. The temperature increase results in a red-shift of λ_0. For the initial ambient temperature, the same wavelength $\lambda_\mathrm{p} = \lambda_0$ can also be achieved by internal heating. The necessary ΔP_diss to create this T_i is labeled with '1' in Fig. 2. Because of the increasing slopes of the $\lambda_\mathrm{p} = \lambda_\mathrm{p}\,(P_\mathrm{diss})$ curves with increasing T_a and the more homogeneous internal temperature profiles for small P_diss we have used temperature steps of only 5°C between the adjacent curves, in contrast to the 20°C step used for illustration in Fig. 2. If we now repeat the procedure for all adjacent curves we get thermal resistances for different T_a that are not constant due to the changing slope of the $\lambda_\mathrm{p} = \lambda_\mathrm{p}(P_\mathrm{diss})$ curves. This is caused by decreasing thermal conductivities of the semiconductor layers with increasing temperature. If we plot the values of R_Th over T_a, as shown in Fig. 3 (right), we get again a linear behavior. The thermal resistance can thus be written as the sum

$$R_\mathrm{Th} = R_\mathrm{Th}(D_\mathrm{ac}) + R_\mathrm{Th}(T_\mathrm{a}) \tag{5}$$

with the contribution $R_\mathrm{Th}(D_\mathrm{ac})$ depending on the semiconductor material and the active diameter and a thermal resistance

$$R_\mathrm{Th}(T_\mathrm{a}) = (T_\mathrm{a} - T_\mathrm{a0}) \cdot \frac{\mathrm{d}R_\mathrm{Th}}{\mathrm{d}T_\mathrm{a}} \tag{6}$$

depending on the ambient temperature, where $R_\mathrm{Th}(D_\mathrm{ac})$ is defined at the temperature $T_\mathrm{a0} = 0°\mathrm{C}$. We find values of $R_\mathrm{Th}(D_\mathrm{ac})$ in the range of $4.54\,\mathrm{K/mW}$ to $3.02\,\mathrm{K/mW}$ and

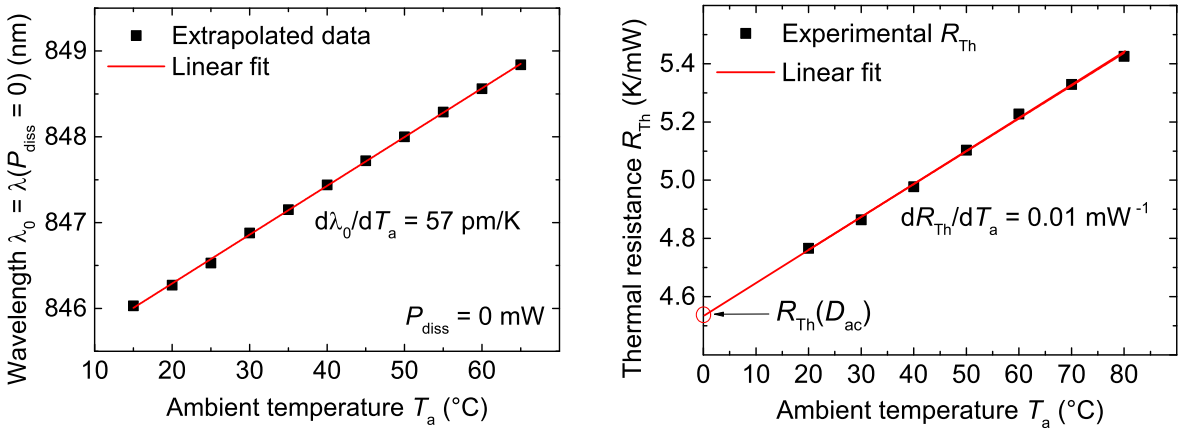

Fig. 3: Intrinsic wavelength λ_0 determined from linear curve fits for different ambient temperatures T_a (left) and extracted thermal resistance R_Th as a function of T_a (right).

$\mathrm{d}R_\mathrm{Th}/\mathrm{d}T_\mathrm{a}$ from $0.0109\,\mathrm{mW}^{-1}$ to $0.0086\,\mathrm{mW}^{-1}$ for active diameters between 4 and 7 µm, respectively.

3. Isothermal Model

As shown in Sect. 2, the proposed analysis of the thermal resistance enables to extract the internal temperature for every point in a LIV curve. This gives the possibility to perform detailed analyses of the thermal effects and extract internal temperature-dependent VCSEL parameters. Furthermore one can also exclude internal heating in the examination of the LIV curves.

For this isothermal model we rearrange the measurement results in a new way. As shown in Fig. 4, we can determine the output power P as a function of T_i for each individual bias current. Similarly from the measured IV characteristic, $V = V(T_\mathrm{a})$ can be plotted for different I. With the help of these data we can now model the isothermal characteristic of the VCSEL for any T_i in the measured range of temperatures. The procedure is visualized in Fig. 4 for $T_\mathrm{i} = 60°\mathrm{C}$. The temperature is kept constant and output powers are collected for every data point. It should be noted that a curve in Fig. 4 can be generated from the experimental data for every intermediate current I. The same procedure is repeated for the IV curve and a LIV diagram is plotted. As a result, in Fig. 5 we find perfectly linear characteristics which strongly deviate from the measured curves. The resulting isothermal LIV curves would be found experimentally for pulsed operation at an ambient temperature $T_\mathrm{a} = T_\mathrm{i}$. For $T_\mathrm{i} = 60°\mathrm{C}$ in Fig. 5 we identify a kink voltage $V_\mathrm{k} = 1.60\,\mathrm{V}$ and a constant differential resistance $R_\mathrm{d} = 109\,\Omega$. The threshold current is $I_\mathrm{th} = 0.45\,\mathrm{mA}$ and the slope efficiency is $\mathrm{SE} = 0.49\,\mathrm{W/A}$. This kind of data evaluation enables us to extract the dependences of I_th, SE, V_k, and R_d on the internal temperature. These are plotted in Fig. 6 for the VCSEL with $D_\mathrm{ac} = 4\,\mu\mathrm{m}$. The data points are fitted with polynomial functions. The threshold current shows a minimum value of $I_\mathrm{th,min} = 0.24\,\mathrm{mA}$ at $T_\mathrm{i} = 5.24°\mathrm{C}$. The threshold minimum nearly corresponds to the maximum achievable slope efficiency $\mathrm{SE}_\mathrm{max} = 0.54\,\mathrm{W/A}$. Both electrical parameters, namely V_k and R_d, decrease

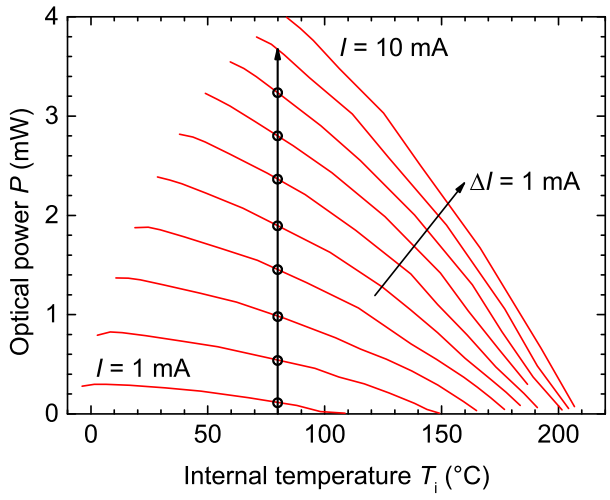

Fig. 4: Optical output power of the VCSEL from Fig. 1 versus internal temperature for different bias currents. The vertical arrow with the open bullets shows how an isothermal $P(I)$ curve is obtained for $T_\mathrm{i} = 60°\mathrm{C}$.

with increasing T_i, as known from the experiment.

4. Conclusion

We have demonstrated a novel approach for the determination of the thermal resistance of vertical-cavity surface-emitting lasers. It is based on measured temperature-dependent continuous-wave light–current–voltage curves and corresponding optical spectra. The analysis requires no empirical data or pulsed measurements. The model allows to calculate the internal temperature at all operating points. Moreover we can simulate an isothermal operation of the VCSEL where the internal temperature is kept constant. As known

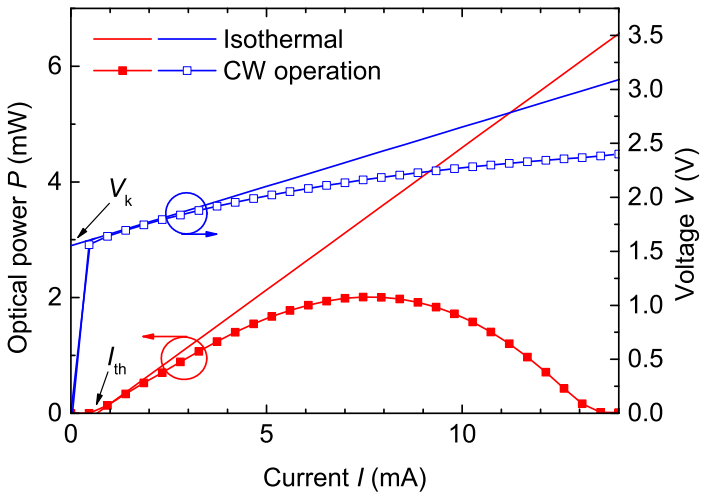

Fig. 5: Comparison of the measured cw output characteristics of a 4 µm VCSEL and isothermal curves for an ambient temperature $T_\mathrm{a} = 60°\mathrm{C}$.

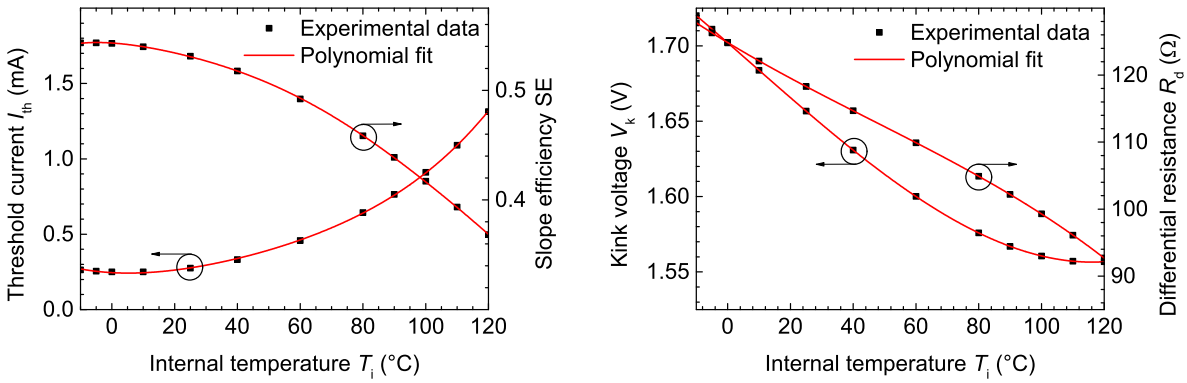

Fig. 6: Threshold current I_{th} and slope efficiency SE on the left as well as kink voltage V_{k} and differential resistance R_{d} on the right, all versus the internal temperature T_{i}.

from laser operation with short electrical pulses, we obtain perfectly linear light–current and current–voltage curves. At the same time, the temperature dependence of the four characteristic laser parameters, namely threshold current, slope efficiency, kink voltage, and differential resistance can be extracted.

Acknowledgment

We thank Philips Technologie GmbH, U-L-M Photonics, Germany for providing the VCSEL material and the measurement setup used in this study, Stefanie Unseld for the data evaluation within her master thesis, and the German Federal Ministry of Education and Research (BMBF) for funding the HyPOT project.

References

[1] K. Jackson and C. Schow, "VCSEL-Based Transceiver for Data Communication," Chap. 14 in *VCSELs*, R. Michalzik (Ed.), pp. 431–448, Springer, Berlin, 2013.

[2] D. Kuchta, "Progress in VCSEL-Based Parallel Links," Chap. 16 in *VCSELs*, R. Michalzik (Ed.), pp. 473–519, Springer, Berlin, 2013.

[3] P. Westbergh, R. Safaisini, E. Haglund, J. Gustavsson, A. Larsson, M. Green, R. Lawrence, and A. Joel, "High-speed oxide confined 850 nm VCSELs operating error-free at 40 Gb/s up to 85°C," *IEEE Photon. Technol. Lett.*, vol. 25, pp. 768–771, 2013.

[4] D. Kuchta, A. Rylyakov, C. Schow, J. Proesel, C. Baks, P. Westbergh, J. Gustavsson, and A. Larsson, "64Gb/s transmission over 57m MMF using an NRZ modulated 850nm VCSEL," *Optical Fiber Commun. Conf. (OFC) 2014*, Th3C.2. San Francisco, CA, USA, Mar. 2014.

[5] D. Mathine, H. Nejad, D. Allee, R. Droopad, and G. Maracas, "Reduction of the thermal impedance of vertical-cavity surface-emitting lasers after integration with copper substrates," *Appl. Phys. Lett.*, vol. 69, pp. 463–464, 1996.

[6] A. AL-Omari and K. Lear, "VCSEL with a self-aligned contact and copper-plated heatsink," *IEEE Photon. Technol. Lett.*, vol. 17, pp. 1767–1769, 2005.

[7] P. Westbergh, J. Gustavsson, B. Kögel, Å. Haglund, and A. Larsson, "Impact of photon lifetime on high-speed VCSEL performance," *IEEE J. Select. Topics Quantum Electron.*, vol. 17, pp. 1603–1613, 2011.

[8] K. Lear and R. Schneider Jr., "Uniparabolic mirror grating for vertical cavity surface emitting lasers," *Appl. Phys. Lett.*, vol. 67, pp. 605–607, 1996.

[9] R. Michalzik, "VCSEL Fundamentals," Chap. 2 in *VCSELs*, R. Michalzik (Ed.), pp. 19–75, Springer, Berlin, 2013.

[10] M. Dabbicco, V. Spagnolo, I. Catalano, and G. Scamarcio, "Direct measurement of the local temperature distribution in oxide VCSELs," in *Vertical-Cavity Surface-Emitting Lasers VI*, C. Lei and S. P. Kilcoyne (Eds.), Proc. SPIE 4649, pp. 62–70, 2002.

[11] E. Kyriakis-Bitzaros and G. Halkias, "Thermal resistance evaluation of high-speed VCSEL: an isothermal optical transient technique," *IEEE Photon. Technol. Lett.*, vol. 14, pp. 269–271, 2002.

[12] P. Debernardi, A. Kroner, F. Rinaldi, and R. Michalzik, "Surface relief versus standard VCSELs: a comparison between experimental and hot-cavity model results," *IEEE J. Select. Topics Quantum Electron.*, vol. 15, pp. 1603–1613, 2009.

[13] P. Baveja, B. Kögel, P. Westbergh, J. Gustavsson, Å. Haglund, D. Maywar, G. Agrawal, and A. Larsson, "Assessment of VCSEL thermal rollover mechanisms from measurements and empirical modeling," *Optics Express*, vol. 19, pp. 15490–15505, 2011.

[14] T. Flick, K. Becks, J. Dopke, P. Mättig, and P. Tegel, "Measurement of the thermal resistance of VCSEL devices," in *Topical Workshop on Electronics for Particle Physics 2010*, doi: 10.1088/1748-0221/6/01/C01021. Aachen, Germany, Sep. 2010.